Loss of Lkb1 and Pten Leads to Lung Squamous Cell Carcinoma with Elevated PD-L1 Expression

Published in final edited form as:
Cancer Cell. 2014 May 12; 25(5): 590–604. doi:10.1016/j.ccr.2014.03.033.

Loss of *Lkb1* and *Pten* Leads to Lung Squamous Cell Carcinoma with Elevated PD-L1 Expression

Chunxiao Xu[1,2,3,15], **Christine M. Fillmore**[4,5,6,15], **Shohei Koyama**[1,7], **Hongbo Wu**[8], **Yanqiu Zhao**[8], **Zhao Chen**[1,2,3], **Grit S. Herter-Sprie**[1,2,3], **Esra A. Akbay**[1,2,3], **Jeremy H. Tchaicha**[1,2,3], **Abigail Altabef**[1,2,3], **Jacob B. Reibel**[1,2,3], **Zandra Walton**[9], **Hongbin Ji**[10], **Hideo Watanabe**[2,14], **Pasi A. Jänne**[1,2,3], **Diego H. Castrillon**[11], **Anil K. Rustgi**[12], **Adam J. Bass**[1,2,14], **Gordon J. Freeman**[2], **Robert F. Padera**[13], **Glenn Dranoff**[1,7], **Peter S. Hammerman**[2,14,*], **Carla F. Kim**[4,5,6,*], and **Kwok-Kin Wong**[1,2,3,*]

[1]Department of Medicine, Harvard Medical School, Boston, MA 02115, USA

[2]Department of Medical Oncology, Dana-Farber Cancer Institute, Boston, MA 02215, USA

[3]Belfer Institute For Applied Cancer Science, Dana-Farber Cancer Institute, Boston, MA 02215, USA

[4]Stem Cell Program, Boston Children's Hospital, Boston, MA 02115, USA

[5]Harvard Stem Cell Institute, Cambridge, MA 02138, USA

[6]Department of Genetics, Harvard Medical School, Boston, MA 02115, USA

[7]Department of Medical Oncology and Cancer Vaccine Center, Dana-Farber Cancer Institute, Boston, MA 02215, USA

[8]Department of Internal Medicine, Henan Cancer Hospital, Affiliated Cancer Hospital of Zhengzhou University, Zhengzhou 450008, China

[9]Abramson Family Cancer Research Institute, Perelman School of Medicine at the University of Pennsylvania, Philadelphia, PA 19104, USA

[10]State Key Laboratory of Cell Biology, Institute of Biochemistry and Cell Biology, Shanghai Institutes for Biological Sciences, Chinese Academy of Sciences, Shanghai 200031, China

[11]Department of Pathology and Simmons Cancer Center, UT Southwestern Medical Center, Dallas, TX 75390, USA

[*]Correspondence: phammerman@partners.org (P.S.H.), carla.kim@childrens.harvard.edu (C.F.K.), kwong1@partners.org (K.-K.W.).
[15]Co-first author

ACCESSION NUMBERS

The Gene Expression Omnibus accession number for the microarray data reported in this paper is GSE54353.

SUPPLEMENTAL INFORMATION

Supplemental Information includes Supplemental Experimental Procedures, seven figures, and four tables and can be found with this article online at http://dx.doi.org/10.1016/j.ccr.2014.03.033.

AUTHOUR CONTRIBUTIONS

C.X. and C.M.F. worked closely on the paper. C.X. and C.M.F. contributed to the experimental design and performed the majority of the experiments. C.X. was responsible primarily for the mouse model establishment and characterization, microenvironment, and immune marker identification. C.M.F. worked primarily on validating the TPC markers in vitro and in vivo, the bioinformatic analysis, and tumor microenvironment characterization. C.X. and C.M.F. contributed to manuscript writing.

[12]Division of Gastroenterology, University of Pennsylvania Perelman School of Medicine, Philadelphia, PA 19104, USA

[13]Department of Pathology, Brigham and Women's Hospital, Boston, MA 02115, USA

[14]Cancer Program, Broad Institute of Harvard and MIT, Cambridge, MA 02142, USA

SUMMARY

Lung squamous cell carcinoma (SCC) is a deadly disease for which current treatments are inadequate. We demonstrate that biallelic inactivation of *Lkb1* and *Pten* in the mouse lung leads to SCC that recapitulates the histology, gene expression, and microenvironment found in human disease. *Lkb1;Pten* null (LP) tumors expressed the squamous markers KRT5, p63 and SOX2, and transcriptionally resembled the basal subtype of human SCC. In contrast to mouse adenocarcinomas, the LP tumors contained immune populations enriched for tumor-associated neutrophils. $SCA1^{+}NGFR^{+}$ fractions were enriched for tumor-propagating cells (TPCs) that could serially transplant the disease in orthotopic assays. TPCs in the LP model and $NGFR^{+}$ cells in human SCCs highly expressed Pd-ligand-1 (PD-L1), suggesting a mechanism of immune escape for TPCs.

INTRODUCTION

Lung squamous cell carcinoma (SCC) is a common type of non-small-cell lung cancer and the second leading cause of death related to lung cancer, causing approximately 400,000 deaths per year worldwide (Cancer Genome Atlas Research Network, 2012; Siegel et al., 2013). Unlike lung adenocarcinoma (ADC), for which many relevant oncogenic mutations have been defined and used to develop strategies for targeted therapies, the genomic landscape of lung SCC is only now emerging. There are not yet any approved targeted therapies for lung SCC. Unfortunately, therapeutic targets in lung ADC, such as *EGFR* and *EML4-ALK*, do not appear to play major roles in lung SCC (Rekhtman et al., 2012). This fact underscores the need to develop a preclinical model of lung SCC in which to define and test novel therapeutic approaches.

Currently, the field lacks a mouse model in which the introduction of genetic alterations found in human squamous lung cancers leads to tumors of purely squamous phenotype. We previously reported that simultaneous activation of $Kras^{G12D}$(*Kras*) and inactivation of *Lkb1* (also known as serine-threonine kinase 11 [*Stk11*]) in the lung gave rise to multiple lung cancer histologies, including SCCs (Ji et al., 2007); however, *KRAS* mutations are very rarely found in human squamous lung tumors. Recently, it was reported that kinase-dead *Ikk*α knockin mice developed spontaneous lung SCCs characterized by *Ikk*α downregulation and marked pulmonary inflammation (Xiao et al., 2013). Significant downregulation of *Lkb1* was found in $Ikk\alpha^{KA/KA}$ lung SCCs and adjacent lung tissues compared with wild-type lungs. Together these results indicate that *Lkb1* reduction is likely an important determinant of lung squamous tumorigenesis.

Despite indications that *Lkb1* loss may be central to the generation of squamous cell cancers, deletion of *Lkb1* alone is unable to drive tumor formation (Ji et al., 2007). *PTEN*

(phosphatase and tensin homolog) is another commonly mutated, deleted, or epigenetically silenced tumor suppressor in human lung cancers (Salmena et al., 2008). Importantly, *PTEN* is altered in 15% of human SCCs (Cancer Genome Atlas Research Network, 2012). PTEN negatively regulates the phosphatidylinositol 3-kinase (PI3K)/AKT pathway, and PI3K pathway gene alterations are found in more than half of human lung SCCs (Cancer Genome Atlas Research Network, 2012). In the mouse model, *Pten* deletion alone in airway basal cells can initiate lung tumor formation, but with low tumor incidence, long latency, and mixed ADC and SCC phenotype (Malkoski et al., 2013).

One key feature of tumor development that autochthonous genetically engineered mouse models provide is a physiologically relevant tumor microenvironment. All of the models of lung SCC to date, including the *Ikkα* knockin mice and a model driven by chronic tuberculosis infection, showed marked pulmonary inflammation (Nalbandian et al., 2009; Xiao et al., 2013), suggesting that an inflammatory microenvironment is central to the development of lung SCCs. This is not surprising given that nearly all humans with lung SCCs have histories of tobacco use that drives squamous metaplasia, and the development of SCCs is associated with inflammatory diseases and chronic immunosuppression. Both tumor-associated macrophages (TAMs) and tumor-associated neutrophils (TANs) comprise significant proportions of the inflammatory infiltrates in a wide variety of mouse tumor models and human cancers (Murdoch et al., 2008). Neutrophils were shown to predominate in human head and neck squamous carcinomas (Trellakis et al., 2011). Neutrophils found in mouse tumors are phenotypically characterized as polymorphonuclear $CD11b^{+}Ly6G^{+}$ cells and may be related to a subtype of myeloid-derived suppressive cells (MDSCs). MDSCs encompass a heterogeneous population of myeloid cells, which share the ability to suppress T cells through the production of arginase, the expression of inducible nitric oxide synthase, and other mechanisms (Dumitru et al., 2012). In the tumor microenvironment, accumulated MDSCs are thought to promote tumor progression through enhancing matrix degradation, tumor cell proliferation, metastasis, and angiogenesis (Welch et al., 1989). MDSCs have also been shown to antagonize effector T cell function, support the generation of immunosuppressive T cell populations, and inhibit the lysis of tumor cells by cytotoxic T cells or natural killer (NK) cells (Dumitru et al., 2012). Some MDSCs have neutrophilic features, but the precise relationship between these cells and normal polymorphonuclear leukocytes remains under active investigation. In this paper, we refer to polymorphonuclear cells infiltrating lung cancers as TANs.

Tumors can also evade immune surveillance by expressing molecules that maintain immune tolerance in peripheral tissues, such as Pd-ligand-1 (PD-L1), which interacts with the immune receptor programmed cell death-1 (PDCD1 or PD-1) (Barber et al., 2006). The PD-1/PD-L1 interaction inhibits $CD8^{+}$ cytotoxic T lymphocyte (CTL) proliferation, survival, and effector function and can induce apoptosis of tumor-infiltrating T cells (Barber et al., 2006); PD-1/PD-L1 interactions can also promote the differentiation of $CD4^{+}$ T cells into $FOXP3^{+}$ Tregs (Francisco et al., 2009), which are known to further suppress the immune system and cause peripheral immune tolerance in lung cancer patients (Adeegbe and Nishikawa, 2013). Ectopic PD-L1 expression in tumor cells in a syngeneic transplant model facilitated the escape of the tumor cells from CTL control (Iwai et al., 2002).

Consistent with these findings in preclinical systems, infusing lung cancer patients with blocking anti-PD-1/PD-L1 monoclonal antibodies has shown efficacy in early stage trials, despite limited activity of prior immunotherapies for lung malignancies (Brahmer et al., 2012; Topalian et al., 2012).

Tumor-propagating cells (TPCs) have the ability to self-renew and differentiate into the bulk population of the tumor and are thought to drive both disease recurrence and metastatic spread (Visvader and Lindeman, 2012). Stem cell antigen-1 (*Sca1* or *Ly6a*) was reported as a bronchioalveolar stem cell (BASC) marker in the distal lung and is also enriched in bronchiolar progenitor cells (Kim et al., 2005; Lee et al., 2014). $SCA1^{+}$ cells, located at the bronchioalveolar duct junction, are hyperproliferative in response to both oncogenic *Kras* and deletion of *Pten*, suggesting that they are susceptible to neoplastic transformation (Kim et al., 2005; Tiozzo et al., 2009). In addition, SCA1 can be used to enrich for TPCs in the lung ADC $Kras^{G12D}$;$p53^{fl/fl}$ (*Kras;p53*) model (Curtis et al., 2010). In the more proximal lung, nerve growth factor receptor (TNFR superfamily, member 16, *Ngfr*) is a stem cell marker for the pseudostratified tracheal epithelium in both human and mouse; NGFR expression is specifically observed in the $p63^{+}$ mouse basal stem cells (Rock et al., 2009). $NGFR^{+}$ basal cells appear to be the cells of origin in a SOX2-induced model of esophageal SCC, and NGFR has been suggested as a putative marker for human esophageal SCC TPCs (Huang et al., 2009; Liu et al., 2013). Despite these clues as to the molecular phenotype of a potential TPC in SCC, no TPC population able to propagate disease serially has been identified for lung SCC.

Using conditional knockout alleles of both *Lkb1* and *Pten*, we found that biallelic inactivation of these two tumor suppressors in the lung resulted in lung tumors with a purely squamous cell phenotype. These squamous lung tumors were 100% penetrant and recapitulated the genetic, molecular, and microenvironmental aspects of the human disease. With this model, the molecular and genetic mechanisms involved in the pathogenesis of lung squamous tumors, including TPCs, microenvironmental factors, immune tolerance, and potential targets for future therapies, can be explored.

RESULTS

$Lkb1^{fl/fl}$;$Pten^{fl/fl}$ Mice Develop Lung SCCs that Recapitulate the Human Disease

In order to examine the possibility that *Lkb1* and *Pten* loss would lead to lung SCC formation, 6- to 8-week-old $Lkb1^{fl/fl}$, $Pten^{fl/fl}$ (*Lkb1*, *Pten* or LP) mice were administered Adenovirus-Cre (Ad-Cre) via intranasal instillation (Figure 1A). In contrast to other lung-specific genetic mouse models described to date, including $Kras^{G12D}$ (*Kras*), $Kras^{G12D}$;$p53^{fl/fl}$ (*Kras;p53*), $Kras^{G12D}$;$Lkb1^{fl/fl}$ (*Kras;Lkb1*), and $Kras^{G12D}$;$p53^{fl/fl}$;$Lkb1^{fl/fl}$ (*Kras;p53;Lkb1*), in which the predominant phenotypes are ADC or mixed adenosquamous cell carcinoma, 100% of the LP mice developed typical lung SCCs with 40 to 50 week latency (Figure 1B; Figures S1A and S1B available online). Small malignant nodules with squamous characteristics were evident at different time points after Ad-Cre infection, ranging from 30 to 40 weeks. Both *Lkb1* and *Pten* were confirmed to be homozygously deleted by PCR on genomic DNA from sorted tumor cells (Figure S1C). The LP tumors were verified as recapitulating human SCC pathology: within the tumor nodules, mature

squamous cells growing in a solid configuration with aberrant nuclear morphology (Figure 1Ca), large infiltrates of neutrophils (Figure 1Cb), and keratinized cells or individual cells with markedly dense eosinophilic cytoplasm were all observed (Figure 1Cc). Tumors showed hallmarks of well-differentiated SCC, including invading fibrous stroma with prominent keratinization (keratin pearls) (Figure 1Cd). In some cases, SCC nodules were visible in airways (Figure 1Ce) and at later time points showed lymphovascular invasion (Figure 1Cf). Tumors arose in both the proximal (Figure S1D, yellow arrow) and distal lung (Figures S1D and S1E, green arrows), though many nodules appeared to be surrounded completely by alveolar epithelium. Low-frequency metastatic lesions were visible in the chest wall of these mice (3 of 78) (Figure S1F).

To confirm the phenotype of the LP tumors, we performed immunohistochemistry (IHC) for markers used clinically to distinguish human lung ADC from lung SCC. *TTF1* (also known as *NKX2-1*) and *SOX2* are genomically amplified in lung ADCs and SCCs, respectively, and routinely used as histologic markers (Bass et al., 2009; Weir et al., 2007). In addition, positive staining for the markers p63 and keratin-5/6 (KRT5/6) appears to robustly differentiate SCCs from ADCs (Fatima et al., 2012). Similar to the human SCC samples, the LP tumor nodules displayed high expression of p63, KRT5, and SOX2, while TTF1 staining was negative (Figure 2A). The expression patterns of p63, KRT5, and SOX2 in SCC colocalized with the expression of epithelial cell adhesion molecule (EpCAM) (Figure 2A). In contrast, *Kras*^{G12D}-driven murine ADC and human ADC tissues were p63, KRT5, and SOX2 negative, while TTF1 staining was strongly positive, confirming their ADC phenotype (Figure 2A). Together these data indicate that LP tumors strongly resemble human SCC by their expression of the classic squamous markers p63, KRT5/6 and SOX2, and hallmarks of squamous differentiation such as keratin deposition.

Next, we compared the transcriptional landscapes of the LP tumors with those found in primary human tumors. To do this, the gene expression profiles of 34 human SCC tumors with either *LKB1* or *PTEN* alterations from the Cancer Genome Atlas (Cancer Genome Atlas Research Network, 2012) were compared with 35 normal human lung tissue samples to generate a list of genotype-specific SCC genes. In parallel, the gene expression profiles of LP tumors from three independent mice were compared with profiles of normal lung from three age-matched LP mice that never received Ad-Cre. In the human comparison, 8,237 genes were significantly differentially expressed in the SCCs versus normal human lung, with a corrected p value (90th percentile false discovery rate) of zero. Compared with normal, 3,658 genes were upregulated in tumors, and 4,579 were downregulated. In the smaller mouse data set, 2,236 genes were differentially expressed, with 916 upregulated and 1,320 downregulated (Figure S2A). Comparison of the mouse and human gene sets yielded 893 genes that were significantly differentially expressed in both human tumors with *LKB1* and/or *PTEN* alterations and LP mouse SCCs (Figure S2B). Among the shared upregulated genes were several known squamous-associated genes, including *SOX2*, *P63*, *NOTCH3*, *HRAS*, and several keratins (*KRT5/KRT6*). Gene ontogeny analysis demonstrated enrichment for genes implicated in squamous differentiation ($p = 3.62 \times 10^{-10}$, Figure 2B). In contrast, the shared downregulated genes were enriched for terminal respiratory unit differentiation,

consistent with the idea that SCC more closely resembles proximal lung cells than distal epithelia ($p = 4.07 \times 10^{-7}$, Figure 2C).

Lkb1$^{fl/fl}$;*Pten*$^{fl/fl}$ Lung SCCs Display Unique Gene Expression, Metabolism, and Downstream Signaling Pathways

In order to characterize the gene expression profiles specific to the tumor cells within the mouse LP SCCs, we used fluorescence-activated cell sorting (FACS) to enrich for the epithelial cells ($CD45^{-}CD31^{-}EpCAM^{+}$) from LP SCC tumor nodules, *Kras*-driven tumor nodules, and normal lung (Figure S3A). We then contrasted the gene expression profiles of these three epithelial cell fractions (Figure 3A, $p < 0.001$). Remarkably, all of the genes differentially expressed between normal epithelial and LP tumor cells were likewise differentially expressed when comparing *Kras* tumor with LP tumor cells. This result suggests that *Kras* tumors retain some gene expression reminiscent of the normal distal lung epithelial cell, from which they likely arise. In contrast, LP tumor cells do not resemble ADC or normal distal lung cells and instead have markers expressed by tracheal basal cells, as discussed below.

We next focused on the genes that were differentially expressed in the LP tumor cells when compared with both *Kras* tumor cells and normal lung. In this comparison, 408 genes were upregulated and 297 genes were downregulated, with a log fold change > 1.8 and an adjusted p value < 0.001 (Table S1). Selected genes that can be organized by function or family are illustrated in a heatmap (Figure 3B). Gene sets that were upregulated in LP tumors include the keratin family members, including *Krt5*, which we observed by IHC, and other squamous keratins such as *Krt6a*, *Krt6b*, and *Krt14*. Also highly upregulated in LP tumors were the transcription factors *Sox2* and *p63*, consistent with our IHC results, and *Slug* and *Pax9*. Among the secreted proteins and cytokines produced by these tumors were several *Cxcl* family members, including *Cxcl3*, *Cxcl7*, and *Cxcl5*, and members of the *Wnt*, *Bmp*, and *interleukin* superfamilies. Several enzymes that were highly expressed in LP cells included *Serpin* family members and *arginase1*. Lastly, genes for proteins and receptors known to be localized to the cell membrane that were highly expressed in LP cells included *Sca1*, *Ngfr*, *Egfr*, and *Pdl1*. *Ngfr* is of particular interest because it is a known stem cell marker in the tracheal epithelium, and *Pdl1* expression suggests a mechanism of immune evasion for LP tumor cells. Genes downregulated in LP tumors included *Tgfrb3* and surfactants.

We next used gene set enrichment analysis (GSEA) to query the pathways and molecular phenotypes specific to the LP tumors (Subramanian et al., 2007). To do this, we queried a rank-ordered gene list comparing LP $EpCAM^{+}$ cells to *Kras* $EpCAM^{+}$ cells for enrichment of the four known transcriptionally defined subclasses of human lung SCC (Wilkerson et al., 2010). We found that the LP model very closely recapitulates the expression pattern found in the basal subtype of human SCC (Figure S3B, $p < 0.0001$, normalized enrichment score [NES] = 1.9). Gene sets enriched in the LP tumor cells compared with *Kras* tumor cells included those positively regulated by AKT1 and mTOR, while a lung-specific KRAS-associated gene set was enriched in the *Kras* cells (Figure S3C; $p < 0.0001$ for AKT1 and mTOR, $p = 0.012$ for KRAS). In addition, compared with tumors driven by *Kras*,

Kras;Lkb1, *Kras;Pten*, and *Kras;p53;Lkb1*, the LP tumors had much stronger p-AKT but weaker p-ERK staining (Figure 3C; Figure S3D). Together these data indicate that the oncogenic signaling pathways activated in the LP tumors predominantly involve AKT and mTOR, whereas those in *Kras* tumors involve downstream mediators of RAS signaling such as MEK and ERK.

To address potential metabolic differences between SCC, ADC, and normal lung, we profiled the metabolites in each tissue. In addition to the transcriptional differences observed among the samples, metabolic profiles of LP tumors, *Kras* tumors, and normal murine lungs were unique. The metabolic profiles of both *Kras* and LP tumors clustered completely separately from normal lung. Furthermore, metabolites in *Kras* tumors and LP tumors segregated the tumor types into two distinct clusters (Figure 3D; Table S2). Among the metabolites most significantly changed in LP cells relative to normal lung were L-arginine (reduced) and creatine (increased) (Figure S3E), which we expected because of the increased expression of *arginase1* in these cells, which we confirmed by real-time RT-PCR (Figure S3F, $p < 0.001$).

Lkb1$^{fl/fl}$;*Pten*$^{fl/fl}$ Lung SCCs Are Enriched for TANs

As noted histologically, the LP SCC lesions contained large neutrophilic infiltrates, suggesting that the immune microenvironment was distinct from the typical TAM-rich microenvironments observed in most mouse *Kras*- and *Kras;p53*-driven ADC models. To better understand the role of the inflammatory microenvironment in lung SCC versus *Kras* ADC, immune cells ($CD45^+$) from LP SCCs and *Kras* or *Kras;p53* ADCs were compared using flow cytometry. In *Kras* and *Kras;p53* tumors, TAMs (alveolar macrophages, $CD45^+CD11c^+CD11b^-CD103^-$) predominated; however, within the LP tumors, the $CD45^+$ population contained significantly fewer macrophages and more TANs ($CD45^+CD11b^+Ly6G^+$) (Figures 4A and 4B, $p < 0.0001$). TANs may promote tumorigenesis by stimulating angiogenesis and immunosuppression in the tumor microenvironment (Dumitru et al., 2013). Interestingly, the prevalence of TANs increased with tumor burden, as lung lobes with higher weight (indicative of higher tumor burden) showed substantially more TANs (Figure 4C, $p < 0.0001$). In contrast, the absolute counts of T cells, B cells, NK cells, and TAMs decreased with increasing lobe weight (Figure S4A), suggesting a selective recruitment and/or proliferation of TANs during SCC tumor progression.

To further confirm the presence of TANs in LP tumor nodules in situ, we performed staining for myeloperoxidase (*Mpo*), a marker that is highly expressed by TANs in tumor-bearing mice (Youn et al., 2012). Within the LP SCCs, MPO^+ TANs appeared to be specifically localized to squamous lesions surrounded by $p63^+$ epithelial cells (Figure 4D; Figure S4B). Conversely, macrophages, identified by $F4/80^+$ staining in mouse tissue, were distributed widely within or around SCC and ADC lesions (Figure 4D; Figure S4B). Similar patterns were observed in human samples; MPO staining was strongly positive in 13 of 15 human primary SCC samples examined, whereas only 4 of 12 human primary ADCs showed staining (Table S3, $p = 0.007$); macrophages ($CD163^+$ in human tissue) were scattered in both human ADCs and SCCs (Figure 4E; Figure S4C). These differences in cell infiltrates

between ADC and SCC lesions were clearly evident in tumors obtained from the mixed histology *p53*$^{fl/fl}$;*Pten*$^{fl/fl}$;*Lkb1*$^{fl/fl}$ (*p53;Lkb1;Pten* or PLP) mouse model. In this model, distinct areas of ADC and SCC were sometimes observed in close proximity in the lung. Confirming their histologic identity, the squamous areas in PLP mice expressed high levels of p63, whereas the acinar areas were negative. Importantly, staining for MPO was specific to the SCC area of the tumor, suggesting that TANs are specifically recruited to SCC lesions (Figure 4F). Similarly, the enrichment for TANs specifically in the areas of SCC tumors but not in the adjacent ADC tumors was also observed in the *Kras;Lkb1* mouse model, which also has the mixed ADC and SCC histology (Figure S4D).

To further explore the differences between CD45$^+$ fractions within SCC and ADC lung tumors, we isolated CD45$^+$EpCAM$^-$ cells from LP and *Kras* tumors and performed microarray analysis. By comparing the gene expression profiles of LP CD45$^+$ cells to LP EpCAM$^+$ cells and *Kras* CD45$^+$ cells, we constructed a list of 156 genes significantly enriched in LP CD45$^+$ cells (Table S4, adjusted $p < 0.025$). Among the genes highly expressed by these cells was *Ly6G*, further confirming the TAN phenotype (Youn et al., 2012). By quantitative PCR, we also confirmed that *Mpo*, *arginase1*, and *Cxcr2* are enriched in SCC lesions from LP mice, whereas their expression was negligible in *Kras*-and *Kras;p53*-tumor derived CD45$^+$ cells ($p = 0.005$, $p < 0.001$, and $p = 0.0011$, respectively; Figure S4E). We then queried immunologic signatures that were enriched in the ranked ordered list of LP versus *Kras* CD45$^+$ genes. By using two sets of independently derived signatures comparing monocyte/macrophages to neutrophils (Abbas et al., 2005; Konuma et al., 2011), we found a clear enrichment for neutrophil signatures in the LP CD45$^+$ cells, while macrophage signatures were significantly enriched in the *Kras* CD45$^+$ cells (Figure 4G) ($p < 0.001$).

Elevated expression of the chemokine receptor *Cxcr2* suggests one mechanism through which the LP EpCAM$^+$ cells are able to specifically recruit TANs. Many of the CXC-ligand family members have neutrophil chemoattractant activity (De Filippo et al., 2013) and appeared to be upregulated at the transcriptional level in our EpCAM microarray. Therefore, we assessed the protein concentrations of these cytokines, including CXCL1, CXCL2, CXCL5, and CXCL7, in bronchoalveolar lavage (BAL) fluid from *Lkb1;Pten* tumor-bearing mice. Compared with levels observed in BAL fluid isolated from normal mice, all these chemokines were significantly elevated in the BAL fluid of LP tumor-bearing mice (Figure S4F, $p < 0.002$), suggesting a mechanism through which TANs are recruited and stimulated by these tumors. In addition, GCSF, another essential regulator of neutrophil trafficking (Semerad et al., 2002), was also elevated in LP BAL fluid (Figure S4F, $p = 0.0002$). Together these data confirm that in contrast to murine *Kras* and *Kras;p53* ADC models that contain predominantly macrophages, lung SCCs show accumulation of TANs, indicating that distinct oncogenic drivers in non-small-cell lung cancer sculpt the immune microenvironment in different ways.

Lkb1$^{fl/fl}$;*Pten*$^{fl/fl}$ Lung SCCs Display Hallmarks of Immune Suppression

We next evaluated the types of T cells present in LP SCC tumors by flow cytometry. Compared with T cell populations isolated from normal lung and peritumoral areas, the T

cells within LP tumors were significantly enriched for Tregs, as determined by FOXP3 staining (Figure 5A). The ratio of $CD8^+$ T cells to $FOXP3^+$ Tregs within the tumor and surrounding tissues decreased with increasing tumor burden, indicating that the levels of immunosuppression rose with disease progression (Figure 5B, $p < 0.0001$). The accumulation of Tregs in LP tumors was further confirmed by immunohistochemical staining for FOXP3 in LP nodules (Figure 5C). In addition, T cells in LP tumors highly expressed the negative T cell costimulatory molecule programmed cell death protein 1 (*PD-1*), and increased percentages of PD-1-positive T cells (both $CD4^+$ and $CD8^+$) correlated with increased tumor burden (Figures 5D and 5E, $p < 0.0001$). In contrast to the increased PD-1 expression on T cells, lymphocyte-activation gene 3 (LAG3) and T cell immunoglobulin domain and mucin domain 3 (TIM3), two other known immune-modulating proteins, showed modestly increased expression (Figure S5A). Cytokines in BAL fluids were further evaluated, including transforming growth factor β (TGF-β) and interleukin-6 (IL-6). Compared with levels in normal lung, these cytokines were significantly increased in BAL fluids from LP tumor-bearing mice (Figure S5B, $p < 0.0009$). Previous reports have shown that TGF-β and IL-6 promote tumor growth, regulate Treg cell development, and cause immunosuppression (Flavell et al., 2010).

Because we observed high levels of *Pdl1* in the LP $EpCAM^+$ cells by microarray, and published work suggests that PD-L1 can induce Tregs (Francisco et al., 2009), we further explored the expression of this immunomodulating protein. PD-L1 expression was first observed on LP tumor cells by IHC (Figure 5F). High cell surface expression of PD-L1 on $EpCAM^+$ $CD45^-$ cells from LP tumors was confirmed by flow cytometry (Figure 5Ga, $p < 0.0001$). We further confirmed the *Pdl1* expression with real-time PCR on $EpCAM^+CD45^-$ cells from normal lung and LP tumors and observed 6-fold more *Pdl1* mRNA in the LP tumor cells compared with levels in normal distal lung epithelium (Figure 5Gb, $p = 0.0013$). The increased numbers of Tregs, together with the high levels of PD-1 and PD-L1 on immune and tumor cells, respectively, indicated that immune suppression may play an important role during lung SCC tumorigenesis.

A $SCA1^+NGFR^+$ Phenotype Is Enriched in *Lkb1*$^{fl/fl}$;*Pten*$^{fl/fl}$ Lung SCC TPCs

We next wished to determine if LP SCCs contained distinct TPC populations. We decided to begin with analysis for two known stem cell makers, SCA1 and NGFR, which mark BASCs and tracheal basal cells, respectively. We first examined NGFR expression on BASCs and SCA1 expression on basal cells. We found that although nearly 100% of $NGFR^+$ basal cells expressed SCA1, only ~25% of $SCA1^+$ BASCs expressed NGFR (Figure S6A). Within the $EpCAM^+CD45^-$ cell populations, LP tumor cells showed high expression of SCA1 and NGFR, and LP tumors harbored a unique population of $SCA1^+NGFR^+$ cells that constituted an average of 17.5% of the LP $EpCAM^+$ cells. Interestingly this population was nearly absent in both *Kras* and *Kras;p53* ADC models (Figures 6A and 6B, $p < 0.0001$; Figures S6B and S6C). *Ngfr* transcript was 30-fold more abundant in LP tumor cells than in normal lung or *Kras* epithelial fractions (Figure S6D, $p < 0.0001$). NGFR also specifically stained the LP SCC tumor lesions but was not detectable in *Kras* tumor lesions by IHC (Figure 6Ca). Likewise, in human primary lung SCCs, NGFR staining was observed in 11 of 13 samples examined, whereas only 2 of 12 human primary ADC sections had detectable

NGFR staining (Figure 6Cb; Table S3; p = 0.001). In PLP tumors in which the ADC and SCC lesions were juxtaposed, NGFR staining was specific to the SCC side of the tissue section (Figure 6Cc).

We next used FACS to fractionate LP EpCAM$^+$CD31$^-$CD45$^-$ tumor cells according to SCA1 and NGFR expression for functional comparison of TPC capacity. First, a surrogate in vitro assay for tumor propagation was used. Four distinct populations, SCA1$^+$NGFR$^+$, SCA1$^-$NGFR$^+$, SCA1$^+$NGFR$^-$, and SCA1$^-$NGFR$^-$ cells, were collected and cocultured in Matrigel (BD Biosciences) with CD45$^+$CD31$^+$ "support" cells isolated from the primary tumors. The tumor colony-forming ability of *Kras* and *Kras;p53* sorted tumor fractions was also evaluated in the 3D Matrigel system (Figure S6E). In agreement with previous in vivo results (Curtis et al., 2010) and validating this assay for TPC capacity, SCA1$^+$ cells from *Kras;p53* tumors were enriched for tumor colony formation ability (p = 0.0026), but the same was not true for *Kras* tumors. SCA1$^+$NGFR$^+$ cells from LP tumors formed the most tumor colonies in 3D cultures, suggesting that they are the fraction enriched for tumor propagation (Figure 6D, p = 0.0011). The morphology and histology of the LP tumor colonies were distinct from those found in *Kras* or *Kras;p53* tumor cultures (Figure S6F). By immunofluorescence, the *Lkb1;Pten* tumor colonies expressed the squamous marker p63 but not the ADC-associated surfactant protein C (SPC), while both the *Kras*- and *Kras;p53*-derived colonies expressed SPC (Figure S6F).

To determine if SCA1$^+$NGFR$^+$ cells from LP tumors were enriched for TPC characteristics in vivo, three major fractions of the EpCAM$^+$ cells from primary LP tumors, SCA1$^+$NGFR$^+$, SCA1$^+$ NGFR$^-$, and SCA1$^-$NGFR$^-$, were transplanted orthotopically into immunocompromised mouse recipients immediately following FACS purification (Figure S6G). The fraction of SCA1$^-$NGFR$^+$ was not tested, because of its reproducibly small abundance. Of the four mice that received SCA1$^+$NGFR$^+$ cells, all developed typical SCC with p63$^+$, SOX2$^+$, and KRT5$^+$ staining within 30 to 40 weeks (Figures 6E and 6F). To assess the presence of self-renewing TPCs within these tumors, the secondary tumors were dissected, dissociated, and sorted for NGFR and SCA1, and the three major fractions were transplanted for tertiary tumor formation. All mice transplanted with SCA1$^+$NGFR$^+$ developed tertiary SCC within 11 to 27 weeks (Figure 6E, p = 0.001 for secondary, p = 0.002 for tertiary, Fisher's exact test). All primary, secondary, and tertiary tumors shared the same histological and FACS characteristics (Figure S6H). Together these data demonstrate that LP tumors contained a distinct population of SCA1$^+$NGFR$^+$ TPCs that could transplant disease retaining squamous characteristics.

TPCs Express High Levels of PD-L1

Little is known about how TPCs escape immunologic clearance and clonally expand to form malignant tumor nodules. To address this question, we further quantified the PD-L1 level on LP tumor cell fractions. By gating the four SCA1;NGFR fractions and analyzing the percentage of PD-L1$^+$ cells in each fraction, we found a clear enrichment for PD-L1$^+$ cells within the SCA1$^+$ NGFR$^+$ fraction (Figure 7A). Within a group of seven mice, an average of 69% of SCA1$^+$NGFR$^+$ cells expressed PD-L1 on their cell surface, whereas only 39% of SCA1$^+$NGFR$^-$ or 32% of SCA1$^-$NGFR$^+$ cells were PD-L1$^+$ (Figure 7B, p = 0.004).

Likewise, by real-time RT-PCR for *Pdl1* within the sorted LP tumor fractions, $SCA1^{+}NGFR^{+}$ cells had 7-fold more *Pdl1* mRNA than $SCA1^{-}NGFR^{-}$ cells and about 2-fold more than $SCA1^{+}NGFR^{-}$ or $SCA1^{-}NGFR^{+}$ cells (Figure 7C, $p = 0.035$). We also used flow cytometry and real-time RT-PCR to assess PD-L1 levels in BASCs and basal cells. $NGFR^{+}$ BASCs expressed the most PD-L1 in the distal lung, while PD-L1 expression was uniformly high by flow cytometry in the trachea (Figures S7A and S7B).

In order to explore the relationship between NGFR and PD-L1 expression in patient tissue, we used human lung SCC tissues that were passaged in immunocompromised mice as patient-derived xenografts (PDXs) (Figure S7C). Hematoxylin and eosin (H&E)-stained sections from the PDX samples showed that the squamous histology of the tumors was retained in the xenograft model (Figure 7D). PDX samples were dissociated and stained with antibodies directed against human CD31, CD45, EpCAM, NGFR, and PD-L1 (Figure S7D). We analyzed the amount of PD-L1 staining on both $EpCAM^{+}NGFR^{+}$ and $EpCAM^{+}NGFR^{-}$ fractions. Using six different PDX samples, PD-L1 staining was 4.2-fold higher in the $NGFR^{+}$ fraction relative to the $NGFR^{-}$ fraction of the human $EpCAM^{+}$ tumor cells (Figure 7E, $p = 0.02$). We further confirmed this trend with independent human lung SCC tumor samples by staining serial sections for NGFR and PD-L1. Clearly, PD-L1 is colocalized to the $NGFR^{+}$ cells within these tumors, indicating that the majority of $NGFR^{+}$ cells coexpress PD-L1 (Figure 7F). Therefore, in lung SCC, PD-L1 is most abundantly expressed on tumor cells that express NGFR, and if these cells are analogous to the $NGFR^{+}$ cells in mouse tumors, they will also be enriched for TPC activity.

DISCUSSION

Here, we demonstrate that biallelic inactivation of both *Lkb1* and *Pten* in the mouse lung leads to fully penetrant SCC. Compared with lung *Kras*-driven ADC models, the immune microenvironment of these SCCs was enriched for TANs. Furthermore, we demonstrate that $SCA1^{+}NGFR^{+}$ tumor cells are enriched for tumor-propagating ability and express high levels of the immune evasion molecule PD-L1. These tumors very closely recapitulate the gene expression profiles of the basal subtype of human lung SCC, indicating that these mice can serve as a valuable model for understanding progression and maintenance of basal lung SCCs. This SCC model will enable the investigation of the molecular mechanisms of human SCC carcinogenesis and will allow further preclinical and coclinical investigation of novel therapies aimed at eradicating lung tumors.

Although lung ADC and SCC occur at relatively equal frequencies worldwide, developing a genetic model of lung SCC has been challenging. The Ad-Cre inhalation method may specifically target more distal lung progenitors, thus selecting for tumor cells of origin that predispose toward an ADC phenotype. Several studies have targeted deletion of squamous tumor suppressors, such as *Pten*, or activation of squamous oncogenes, such as *Sox2*, but despite these efforts, only partial SCC differentiation was observed in either model (Lu et al., 2010; Malkoski et al., 2013). Here, we demonstrate that deletion of both *Pten* and *Lkb1*, via the traditional Ad-Cre inhalation system, is able to produce lung tumors of purely squamous phenotype. *Lkb1;Pten* tumor lesions appeared to grow into the distal lung, suggesting that if basal cells are the cells of origin, they are able to migrate more distally to

propagate disease. When we examined the expression of stem cell markers in normal lung tissue, 100% of basal cells were $SCA1^+$, while ~25% of BASCs were $NGFR^+$. These data suggest an alternative possibility that a rare subset of $NGFR^+$ BASCs could serve as distal cells of origin for these tumors. Surfactant protein C Cre-recombinase and club cell secretory protein Cre-recombinase both failed to produce tumors when used with the *Lkb1;Pten* alleles (data not shown), indicating that distal lung cells may not be the primary targets of oncogenic transformation in this model. Further examination of the cells of origin for these tumors, including the use of basal cell-specific Cre strains or repetitive injury that targets particular cell populations, will help us understand which lung cells can serve as precursors for these squamous tumors.

As expected, the loss of both *Lkb1* and *Pten* in these tumors activated the AKT and mTOR pathways, likely driving cellular proliferation and tumorigenesis. The deletion of these genes was also associated with the upregulation of specific cytokines and other immune-modulating proteins, leading to a unique tumor microenvironment. Compared with *Kras* tumor cells, the LP $EpCAM^+$ cells expressed very high levels of the chemokines CXCL3 and CXCL5, and the BAL fluid contained elevated CXCL1, CXCL2, CXCL5, and CXCL7. The CXC chemokine family controls the migration and adhesion of monocytes and neutrophils, mediating its effects on target cells by interacting with CXCR2 (Põld et al., 2004). CXCL5 is also known as epithelial-derived neutrophil-activating peptide 78, and its expression is associated with PI3K/AKT and Raf/MEK/ERK activation (Hsu et al., 2013). Recent findings in tumor-bearing mice and cancer patients indicate that the increased metabolism of L-arginine by TANs producing arginase1 can inhibit T cell lymphocyte responses (Raber et al., 2012), and it is likely that this mechanism is in play in the LP tumors. Furthermore, we observed strong MPO staining in patient SCC tissues, suggesting that activated TANs are a key component of SCC in both mouse and human.

In addition to expression of the TAN-attracting cytokines, the LP $EpCAM^+$ cells expressed high levels of the immune evasion molecule PD-L1. Recently, there has been much excitement surrounding the potential of targeting molecules such as PD-L1 to “reawaken” the immune system and cause tumor destruction. In the phase 1 study of nivolumab, a fully humanized monoclonal antibody to PD-1, PD-L1 expression was determined by IHC in pretreatment tumor biopsies of various tumor types (n = 42). Thirty-six percent of patients whose tumors showed PD-L1 expression achieved objective response to nivolumab treatment (9 of 25), while none of the 17 patients with PD-L1-negative tumors showed any objective response, although some achieved prolonged stable disease (Topalian et al., 2012). These data indicate that PD-L1 expression might influence response to anti-PD-1 antibody therapy. With the accumulation of clinical data, the actual correlation between PD-L1 expression and response to anti-PD-1 therapy should become clearer.

Intriguingly, the TPCs within our SCC model showed enrichment for PD-L1 expression, suggesting that TPCs have unique immune evasion properties. Strikingly, we found that the $SCA1^+NGFR1^+$ cell population had enhanced tumor-propagating activity compared with other tumor cell populations. Notably, our studies compared three tumor cell populations from murine SCC, but the $SCA1^-NGFR^+$ population could not be assessed because of low abundance. Thus, there could be additional TPCs to characterize in *Lkb1;Pten* SCCs.

Furthermore, although PDX analyses showed that $NGFR^+$ human SCC cells are enriched for PD-L1, we have not yet established the identity of TPCs in human SCC with a functional assay. SCA1 as a TPC marker is not useful for human cell studies, and markers in addition to NGFR may be required to enrich for propagating activity from primary patient SCCs. It is also currently unclear how universal the immune evasion ability of TPCs we found will be in human SCC or in other tissues. It will be crucial in future studies to investigate TPCs in other tumor types and characterize their PD-L1 expression to further explore this intriguing link between immune escape and tumor propagation. In the future, it may be possible to first debulk the tumor with a more generally targeted inhibitor or surgery and then prevent tumor recurrence and/or metastasis through administration of anti-PD-1 therapy to target TPCs. Together these data demonstrate the potential of immunotherapy for the treatment of lung SCC and lay the groundwork for further investigation into the response of both cancer cells and the immune microenvironment to such treatments.

EXPERIMENTAL PROCEDURES

Mouse Cohorts and Human Samples

All mice were housed in a biosafety level 2 lab at Dana-Farber Cancer Institute. All care and treatment of experimental animals were in accordance with Harvard Medical School/Dana-Farber Cancer Institute institutional animal care and use committee guidelines. Detailed mouse cohort information can be found in Supplemental Experimental Procedures. Patient slides were provided by the Pathology Department of Brigham and Women's Hospital. The human samples were obtained from consented subjects at the Dana-Farber Cancer Institute/Harvard Cancer Center under institutional review board-approved protocol 02-180. Frozen PDX tissues were purchased from the Van Andel Institute.

Flow Cytometry Analysis and Sorting

Tumors were dissected from the lungs of primary mice, and tumor tissue was prepared as previously described (Curtis et al., 2010). Single-cell suspensions were stained using rat-antimouse antibodies. Detailed antibody information and gating strategy can be found in Supplemental Experimental Procedures.

3D Culture and Tumor Transplants

FACS-sorted mouse cells were resuspended in MTEC/Plus containing 20 ng/ml EGF and FGF2, mixed 1:1 with growth factor-reduced Matrigel, and pipetted into a 12-well 0.4 μm Transwell insert (Falcon). MTEC/Plus medium (700 μl) was added to the lower chamber and refreshed every other day. Intratracheal transplantation was performed as previously described (Curtis et al., 2010). Intrathoracic injections were performed as previously described (Jongsma et al., 2008).

Metabolomics Profiles Analysis

Metabolite extraction and targeted mass spectrometry analysis for metabolomics profiles were conducted as reported previously (Yuan et al., 2012). Briefly, the frozen tumors were smashed in cold 80% high-performance liquid chromatography-grade methanol on dry ice twice, and then the extractions were Speed Vac/lyophilized to a pellet using no heat. The

data were normalized and analyzed with MetaboAnalyst 2.0 (Xia et al., 2012). In hierarchical cluster analysis, each sample begins as a separate cluster, and the algorithm proceeds to combine them until all samples belong to one cluster. Clustering results are shown as heatmap (distance measure using Pearson and clustering algorithm using Ward).

Statistical Analysis

Statistical analyses were carried out using GraphPad Prism (GraphPad Software). All numerical data are presented as mean ± SEM. Grouped analysis was performed using two-way ANOVA. Column analysis was using one-way ANOVA or Student's t test. A p value < 0.05 was considered statistically significant.

Supplementary Material

Refer to Web version on PubMed Central for supplementary material.

Acknowledgments

We thank the Boston Children's Hospital flow cytometry facility and members of the C.F.K. and Zon Labs for helpful discussions. This work was supported in part by the United Against Lung Cancer and the Susan Spooner Research Fund (to K.-K.W.); American Cancer Society Post-Doctoral Fellowship PF-12-151-01-DMC (to C.M.F.); a Margaret A. Cunningham Immune Mechanisms in Cancer Research Fellowship Award (to S.K.); American Cancer Society Research Scholar grant RSG-08-082-01-MGO, the V Foundation for Cancer Research, a Basil O'Conner March of Dimes Starter Award, the Harvard Stem Cell Institute, and the Lung Cancer Research Foundation (to C.F.K.); the Cancer Prevention Research Institute of Texas (RP100550); and grants HL090136, HL100402, CA122794, CA140594, CA163896, CA166480, P0CA154303, CA098101, CA141576, CA137181, P0CA120964, CA143083, and CA163677 from the NIH.

References

Abbas AR, Baldwin D, Ma Y, Ouyang W, Gurney A, Martin F, Fong S, van Lookeren Campagne M, Godowski P, Williams PM, et al. Immune response in silico (IRIS): immune-specific genes identified from a compendium of microarray expression data. Genes Immun. 2005; 6:319–331. [PubMed: 15789058]

Adeegbe DO, Nishikawa H. Natural and induced T regulatory cells in cancer. Front Immunol. 2013; 4:190. [PubMed: 23874336]

Barber DL, Wherry EJ, Masopust D, Zhu B, Allison JP, Sharpe AH, Freeman GJ, Ahmed R. Restoring function in exhausted CD8 T cells during chronic viral infection. Nature. 2006; 439:682–687. [PubMed: 16382236]

Bass AJ, Watanabe H, Mermel CH, Yu S, Perner S, Verhaak RG, Kim SY, Wardwell L, Tamayo P, Gat-Viks I, et al. SOX2 is an amplified lineage-survival oncogene in lung and esophageal squamous cell carcinomas. Nat Genet. 2009; 41:1238–1242. [PubMed: 19801978]

Brahmer JR, Tykodi SS, Chow LQ, Hwu WJ, Topalian SL, Hwu P, Drake CG, Camacho LH, Kauh J, Odunsi K, et al. Safety and activity of anti-PD-L1 antibody in patients with advanced cancer. N Engl J Med. 2012; 366:2455–2465. [PubMed: 22658128]

Cancer Genome Atlas Research Network. Comprehensive genomic characterization of squamous cell lung cancers. Nature. 2012; 489:519–525. [PubMed: 22960745]

Curtis SJ, Sinkevicius KW, Li D, Lau AN, Roach RR, Zamponi R, Woolfenden AE, Kirsch DG, Wong KK, Kim CF. Primary tumor genotype is an important determinant in identification of lung cancer propagating cells. Cell Stem Cell. 2010; 7:127–133. [PubMed: 20621056]

De Filippo K, Dudeck A, Hasenberg M, Nye E, van Rooijen N, Hartmann K, Gunzer M, Roers A, Hogg N. Mast cell and macrophage chemokines CXCL1/CXCL2 control the early stage of neutrophil recruitment during tissue inflammation. Blood. 2013; 121:4930–4937. [PubMed: 23645836]

Dumitru CA, Moses K, Trellakis S, Lang S, Brandau S. Neutrophils and granulocytic myeloid-derived suppressor cells: immunophenotyping, cell biology and clinical relevance in human oncology. Cancer Immunol Immunother. 2012; 61:1155–1167. [PubMed: 22692756]

Dumitru CA, Lang S, Brandau S. Modulation of neutrophil granulocytes in the tumor microenvironment: mechanisms and consequences for tumor progression. Semin Cancer Biol. 2013; 23:141–148. [PubMed: 23485549]

Fatima N, Cohen C, Lawson D, Siddiqui MT. Combined double CK5/P63 stain: useful adjunct test for diagnosing pulmonary squamous cell carcinoma. Diagn Cytopathol. 2012; 40:943–948. [PubMed: 21472873]

Flavell RA, Sanjabi S, Wrzesinski SH, Licona-Limón P. The polarization of immune cells in the tumour environment by TGFbeta. Nat Rev Immunol. 2010; 10:554–567. [PubMed: 20616810]

Francisco LM, Salinas VH, Brown KE, Vanguri VK, Freeman GJ, Kuchroo VK, Sharpe AH. PD-L1 regulates the development, maintenance, and function of induced regulatory T cells. J Exp Med. 2009; 206:3015–3029. [PubMed: 20008522]

Hsu YL, Hou MF, Kuo PL, Huang YF, Tsai EM. Breast tumor-associated osteoblast-derived CXCL5 increases cancer progression by ERK/MSK1/Elk-1/Snail signaling pathway. Oncogene. 2013; 32:4436–4447. [PubMed: 23045282]

Huang SD, Yuan Y, Liu XH, Gong DJ, Bai CG, Wang F, Luo JH, Xu ZY. Self-renewal and chemotherapy resistance of p75NTR positive cells in esophageal squamous cell carcinomas. BMC Cancer. 2009; 9:9. [PubMed: 19134212]

Iwai Y, Ishida M, Tanaka Y, Okazaki T, Honjo T, Minato N. Involvement of PD-L1 on tumor cells in the escape from host immune system and tumor immunotherapy by PD-L1 blockade. Proc Natl Acad Sci U S A. 2002; 99:12293–12297. [PubMed: 12218188]

Ji H, Ramsey MR, Hayes DN, Fan C, McNamara K, Kozlowski P, Torrice C, Wu MC, Shimamura T, Perera SA, et al. LKB1 modulates lung cancer differentiation and metastasis. Nature. 2007; 448:807–810. [PubMed: 17676035]

Jongsma J, van Montfort E, Vooijs M, Zevenhoven J, Krimpenfort P, van der Valk M, van de Vijver M, Berns A. A conditional mouse model for malignant mesothelioma. Cancer Cell. 2008; 13:261–271. [PubMed: 18328429]

Kim CF, Jackson EL, Woolfenden AE, Lawrence S, Babar I, Vogel S, Crowley D, Bronson RT, Jacks T. Identification of bronchioalveolar stem cells in normal lung and lung cancer. Cell. 2005; 121:823–835. [PubMed: 15960971]

Konuma T, Nakamura S, Miyagi S, Negishi M, Chiba T, Oguro H, Yuan J, Mochizuki-Kashio M, Ichikawa H, Miyoshi H, et al. Forced expression of the histone demethylase Fbxl10 maintains self-renewing hematopoietic stem cells. Exp Hematol. 2011; 39:697–709.e5. [PubMed: 21540074]

Lee JH, Bhang DH, Beede A, Huang TL, Stripp BR, Bloch KD, Wagers AJ, Tseng YH, Ryeom S, Kim CF. Lung stem cell differentiation in mice directed by endothelial cells via a BMP4-NFATc1-thrombospondin-1 axis. Cell. 2014; 156:440–455. [PubMed: 24485453]

Liu K, Jiang M, Lu Y, Chen H, Sun J, Wu S, Ku WY, Nakagawa H, Kita Y, Natsugoe S, et al. Sox2 cooperates with inflammation-mediated Stat3 activation in the malignant transformation of foregut basal progenitor cells. Cell Stem Cell. 2013; 12:304–315. [PubMed: 23472872]

Lu Y, Futtner C, Rock JR, Xu X, Whitworth W, Hogan BL, Onaitis MW. Evidence that SOX2 overexpression is oncogenic in the lung. PLoS ONE. 2010; 5:e11022. [PubMed: 20548776]

Malkoski, SP.; Cleaver, TG.; Thompson, JJ.; Sutton, WP.; Haeger, SM.; Rodriguez, KJ.; Lu, SL.; Merrick, D.; Wang, XJ. Role of PTEN in basal cell derived lung carcinogenesis. Mol Carcinog. 2013. Published online April 26, 2013 http://dx.doi.org/10.1002/mc.22030

Murdoch C, Muthana M, Coffelt SB, Lewis CE. The role of myeloid cells in the promotion of tumour angiogenesis. Nat Rev Cancer. 2008; 8:618–631. [PubMed: 18633355]

Nalbandian A, Yan BS, Pichugin A, Bronson RT, Kramnik I. Lung carcinogenesis induced by chronic tuberculosis infection: the experimental model and genetic control. Oncogene. 2009; 28:1928–1938. [PubMed: 19330024]

Põld M, Zhu LX, Sharma S, Burdick MD, Lin Y, Lee PP, Põld A, Luo J, Krysan K, Dohadwala M, et al. Cyclooxygenase-2-dependent expression of angiogenic CXC chemokines ENA-78/CXC ligand

(CXCL) 5 and interleukin-8/CXCL8 in human non-small cell lung cancer. Cancer Res. 2004; 64:1853–1860. [PubMed: 14996749]

Raber P, Ochoa AC, Rodríguez PC. Metabolism of L-arginine by myeloid-derived suppressor cells in cancer: mechanisms of T cell suppression and therapeutic perspectives. Immunol Invest. 2012; 41:614–634. [PubMed: 23017138]

Rekhtman N, Paik PK, Arcila ME, Tafe LJ, Oxnard GR, Moreira AL, Travis WD, Zakowski MF, Kris MG, Ladanyi M. Clarifying the spectrum of driver oncogene mutations in biomarker-verified squamous carcinoma of lung: lack of EGFR/KRAS and presence of PIK3CA/AKT1 mutations. Clin Cancer Res. 2012; 18:1167–1176. [PubMed: 22228640]

Rock JR, Onaitis MW, Rawlins EL, Lu Y, Clark CP, Xue Y, Randell SH, Hogan BL. Basal cells as stem cells of the mouse trachea and human airway epithelium. Proc Natl Acad Sci U S A. 2009; 106:12771–12775. [PubMed: 19625615]

Salmena L, Carracedo A, Pandolfi PP. Tenets of PTEN tumor suppression. Cell. 2008; 133:403–414. [PubMed: 18455982]

Semerad CL, Liu F, Gregory AD, Stumpf K, Link DC. G-CSF is an essential regulator of neutrophil trafficking from the bone marrow to the blood. Immunity. 2002; 17:413–423. [PubMed: 12387736]

Siegel R, Naishadham D, Jemal A. Cancer statistics, 2013. CA Cancer J Clin. 2013; 63:11–30. [PubMed: 23335087]

Subramanian A, Kuehn H, Gould J, Tamayo P, Mesirov JP. GSEA-P: a desktop application for gene set enrichment analysis. Bioinformatics. 2007; 23:3251–3253. [PubMed: 17644558]

Tiozzo C, De Langhe S, Yu M, Londhe VA, Carraro G, Li M, Li C, Xing Y, Anderson S, Borok Z, et al. Deletion of Pten expands lung epithelial progenitor pools and confers resistance to airway injury. Am J Respir Crit Care Med. 2009; 180:701–712. [PubMed: 19574443]

Topalian SL, Hodi FS, Brahmer JR, Gettinger SN, Smith DC, McDermott DF, Powderly JD, Carvajal RD, Sosman JA, Atkins MB, et al. Safety, activity, and immune correlates of anti-PD-1 antibody in cancer. N Engl J Med. 2012; 366:2443–2454. [PubMed: 22658127]

Trellakis S, Bruderek K, Dumitru CA, Gholaman H, Gu X, Bankfalvi A, Scherag A, Hütte J, Dominas N, Lehnerdt GF, et al. Polymorphonuclear granulocytes in human head and neck cancer: enhanced inflammatory activity, modulation by cancer cells and expansion in advanced disease. Int J Cancer. 2011; 129:2183–2193. [PubMed: 21190185]

Visvader JE, Lindeman GJ. Cancer stem cells: current status and evolving complexities. Cell Stem Cell. 2012; 10:717–728. [PubMed: 22704512]

Weir BA, Woo MS, Getz G, Perner S, Ding L, Beroukhim R, Lin WM, Province MA, Kraja A, Johnson LA, et al. Characterizing the cancer genome in lung adenocarcinoma. Nature. 2007; 450:893–898. [PubMed: 17982442]

Welch DR, Schissel DJ, Howrey RP, Aeed PA. Tumor-elicited polymorphonuclear cells, in contrast to “normal” circulating polymorphonuclear cells, stimulate invasive and metastatic potentials of rat mammary adenocarcinoma cells. Proc Natl Acad Sci U S A. 1989; 86:5859–5863. [PubMed: 2762301]

Wilkerson MD, Yin X, Hoadley KA, Liu Y, Hayward MC, Cabanski CR, Muldrew K, Miller CR, Randell SH, Socinski MA, et al. Lung squamous cell carcinoma mRNA expression subtypes are reproducible, clinically important, and correspond to normal cell types. Clin Cancer Res. 2010; 16:4864–4875. [PubMed: 20643781]

Xia J, Mandal R, Sinelnikov IV, Broadhurst D, Wishart DS. MetaboAnalyst 2.0—a comprehensive server for metabolomic data analysis. Nucleic Acids Res. 2012; 40(Web Server issue):W127–W133. [PubMed: 22553367]

Xiao Z, Jiang Q, Willette-Brown J, Xi S, Zhu F, Burkett S, Back T, Song NY, Datla M, Sun Z, et al. The pivotal role of IKKα in the development of spontaneous lung squamous cell carcinomas. Cancer Cell. 2013; 23:527–540. [PubMed: 23597566]

Youn JI, Collazo M, Shalova IN, Biswas SK, Gabrilovich DI. Characterization of the nature of granulocytic myeloid-derived suppressor cells in tumor-bearing mice. J Leukoc Biol. 2012; 91:167–181. [PubMed: 21954284]

Yuan M, Breitkopf SB, Yang X, Asara JM. A positive/negative ion-switching, targeted mass spectrometry-based metabolomics platform for bodily fluids, cells, and fresh and fixed tissue. Nat Protoc. 2012; 7:872–881. [PubMed: 22498707]

Significance

Although many of the molecular alterations underlying human lung SCC were recently described, lung SCC has been challenging to model in the mouse, and there are few in vivo models for the development of novel cancer therapeutics for this disease. The SCC model described herein is an important tool for investigating the molecular mechanisms of SCC carcinogenesis, including the identity of TPCs and the involvement of the immune microenvironment in tumor progression. This model also provides a platform to study new therapeutic opportunities for lung SCC through the targeting of a TPC-specific interaction with the immune cell microenvironment.

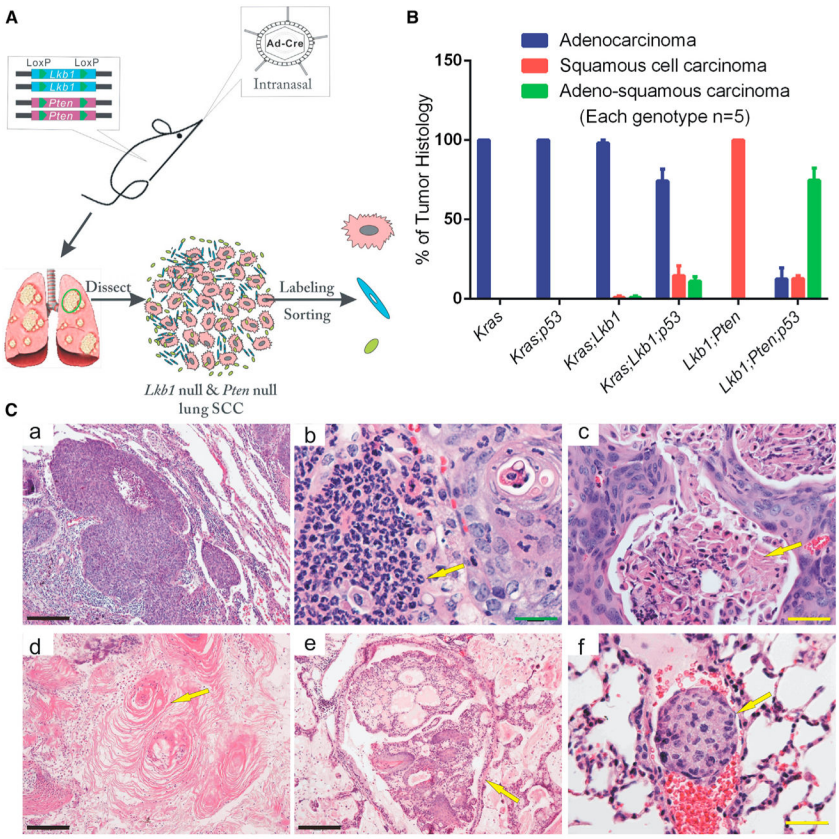

Figure 1. Biallelic Inactivation of Both *Lkb1* and *Pten* in the Mouse Lung Leads to SCC

(A) Schematic of biallelic inactivation of both *Lkb*1 and *Pten* in the mouse lung by Ad-Cre inhalation, followed by tumor dissociation and sorting.

(B) Phenotypic quantification of lung tumor histologies from the indicated conditional mouse models, including *Kras*^{G12D} (*Kras*), *Kras*^{G12D};*p53*$^{fl/fl}$ (*Kras;p53*), *Kras*^{G12D};*Lkb1*$^{fl/fl}$ (*Kras;Lkb1*), and *Kras*^{G12D};*p53*$^{fl/fl}$;*Lkb1*$^{fl/fl}$ (*Kras;p53;Lkb1*), *Lkb1*$^{fl/fl}$;*Pten*$^{fl/fl}$ (*Lkb1*, *Pten*) *Lkb1*$^{fl/fl}$;*Pten*$^{fl/fl}$;*p53*$^{fl/fl}$ (*Lkb1;Pten;p53*), which all rely upon Ad-Cre inhalation for tumor initiation (mean ± SEM, n = 5 mice per genotype).

(C) Representative H&E-stained sections derived from tumors arising in the *Lkb1;Pten* mouse model. Yellow arrows indicate specific features on individual images. (a) Mature squamous cells with aberrant nuclear morphology; (b) large infiltrates of neutrophils in SCC nodules; (c) keratinized cells with markedly dense eosinophilic cytoplasm surrounded by epithelial cells; (d) well-differentiated SCC with keratin pearls; (e) SCC nodules in large airways; (f) squamous-like tumor cell lymphovascular invasion.

Black scale bars represent 200 μm, yellow scale bars represent 50 μm, and the green scale bar represents 25 μm. See also Figure S1.

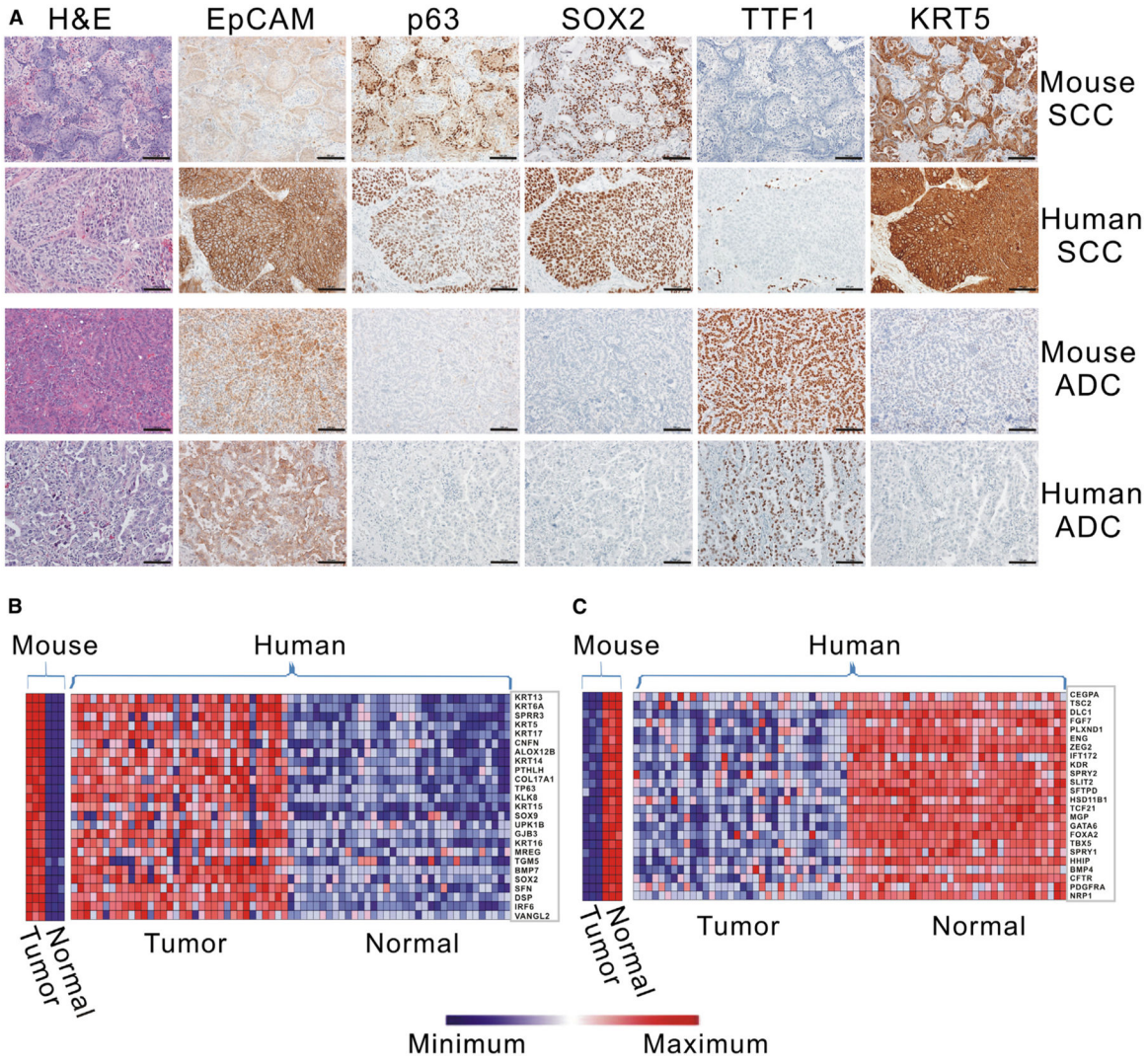

Figure 2. Lung SCCs in *Lkb1*$^{fl/fl}$;*Pten*$^{fl/fl}$ Mice Closely Recapitulated the Human Disease

(A) Immunohistochemically stained human and mouse ADC and SCC tumors. The SCC canonical markers KRT5, SOX2, and p63 and the ADC canonical marker TTF1 were used to distinguish the tumor types. EpCAM is an epithelial cell marker, and the expression patterns of p63, KRT5, and SOX2 in SCC colocalized with EpCAM expression. Scale bars represent 100 μm for all panels.

(B) Microarray expression profiling of normal lung and SCC tumors from mouse and human (see description in text). Upregulated genes in both mouse and human SCC were enriched for a squamous differentiation signature.

(C) Downregulated genes from the analysis in (B) were enriched for a normal lung terminal respiratory unit signature. See also Figure S2.

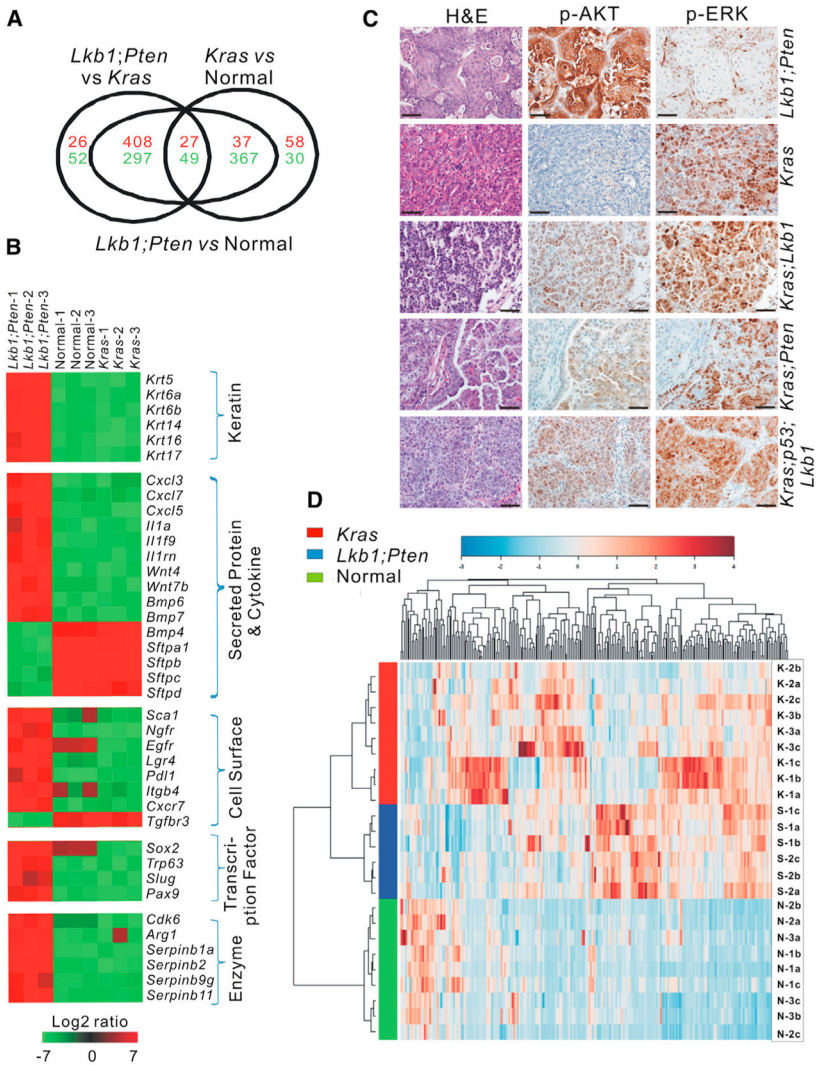

Figure 3. *Lkb1*$^{fl/fl}$;*Pten*$^{fl/fl}$ Lung SCCs Display Unique Gene Expression, Metabolism, and Downstream Signaling Pathways

(A) EpCAM^{+}CD31^{-}CD45^{-} cells were isolated by FACS and subject to microarray expression analysis. Euler diagram illustrating the gene expression profiles of epithelial cells from LP SCCs, *Kras* ADCs, and normal lung tissues.

(B) Heatmap depicting differential expression of selected genes in LP SCCs, *Kras* ADCs, and normal lung tissues as determined by microarray expression profiling. Red indicates upregulation. and green indicates downregulation.

(C) Immunohistochemical staining for p-AKT and p-ERK on LP, *Kras*, *Kras;Lkb1*, *Kras;Pten*, and *Kras;p53;Lkb1* tumor nodules. Scale bars represent 50 μm for all panels.

(D) Hierarchical clustering by Ward method of quantitative metabolomic profiling for LP SCC tumors (S), *Kras* ADC tumors (K), and normal lung tissues (N).

See also Figure S3 and Tables S1 and S2.

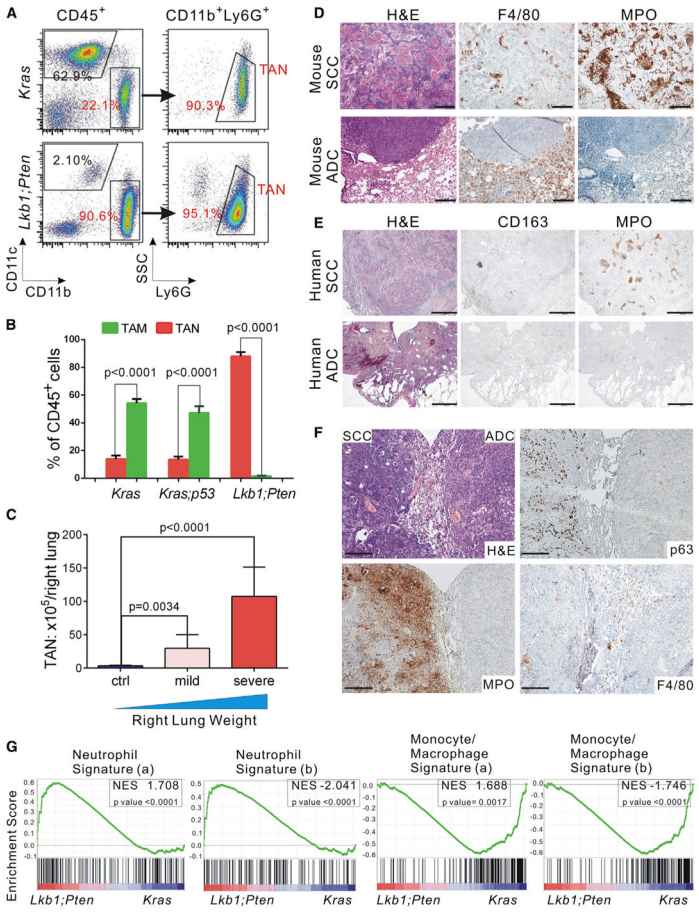

Figure 4. TANs Were the Predominant Inflammatory Cell Population in *Lkb1*$^{fl/fl}$;*Pten*$^{fl/fl}$ SCC Tumors

(A) Representative flow cytometry plots for *Kras* ADC and LP SCC dissociated tumors. Plots are gated on live single CD45$^+$ cells. In *Kras* tumors, tumor TAMs (CD45$^+$CD11c$^+$CD11b$^-$CD103$^-$) constituted the majority of CD45$^+$ cells, whereas in LP tumors, TANs (CD45$^+$CD11b$^+$Ly6G$^+$) were predominant. Gating strategies are also described in Experimental Procedures.

(B) Quantification of inflammatory cell populations in *Kras* tumors (n = 7), *Kras;p53* tumors (n = 8), and *Lkb1;Pten* tumors (n = 7) by flow cytometry (mean ± SEM, $p < 0.0001$).

(C) Quantification of TANs within right lung lobes from samples with progressively increasing weights (shown in Figure S4A), indicating different tumor burdens: n = 8 for normal lung control (ctrl), n = 5 for mild disease group (tumor plus surrounding tissue weight < 750 mg), n = 5 for severe disease group (tumor plus surrounding tissue weight > 750 mg) (mean ± SEM; mild versus control $p = 0.0034$, severe versus control $p < 0.0001$).

(D and E) Representative immunohistochemical staining for MPO, F4/80 (D), and CD163 (E) in SCCs and ADCs; the mouse slides were LP SCC and *Kras*-driven ADCs. MPO staining indicating neutrophils was positive only in SCC nodules. F4/80 marks macrophages in mice (D), while CD163 marks macrophages in humans (E). Scale bars represent 200 μm for all panels of (D) and 800 μm for all panels of (E).

(F) Representative immunohistochemical staining on *Lkb1;Pten;p53* tumors in which distinct areas of ADC and SCC were adjacently located. p63 and MPO staining was restricted to the SCC area. Scale bars represent 200 μm for all panels.
(G) GSEA was used to confirm the major immune cell types within *Lkb1;Pten* SCCs and *Kras* ADCs (Abbas et al., 2005; Konuma et al., 2011). See also Figure S4 and Tables S3 and S4.

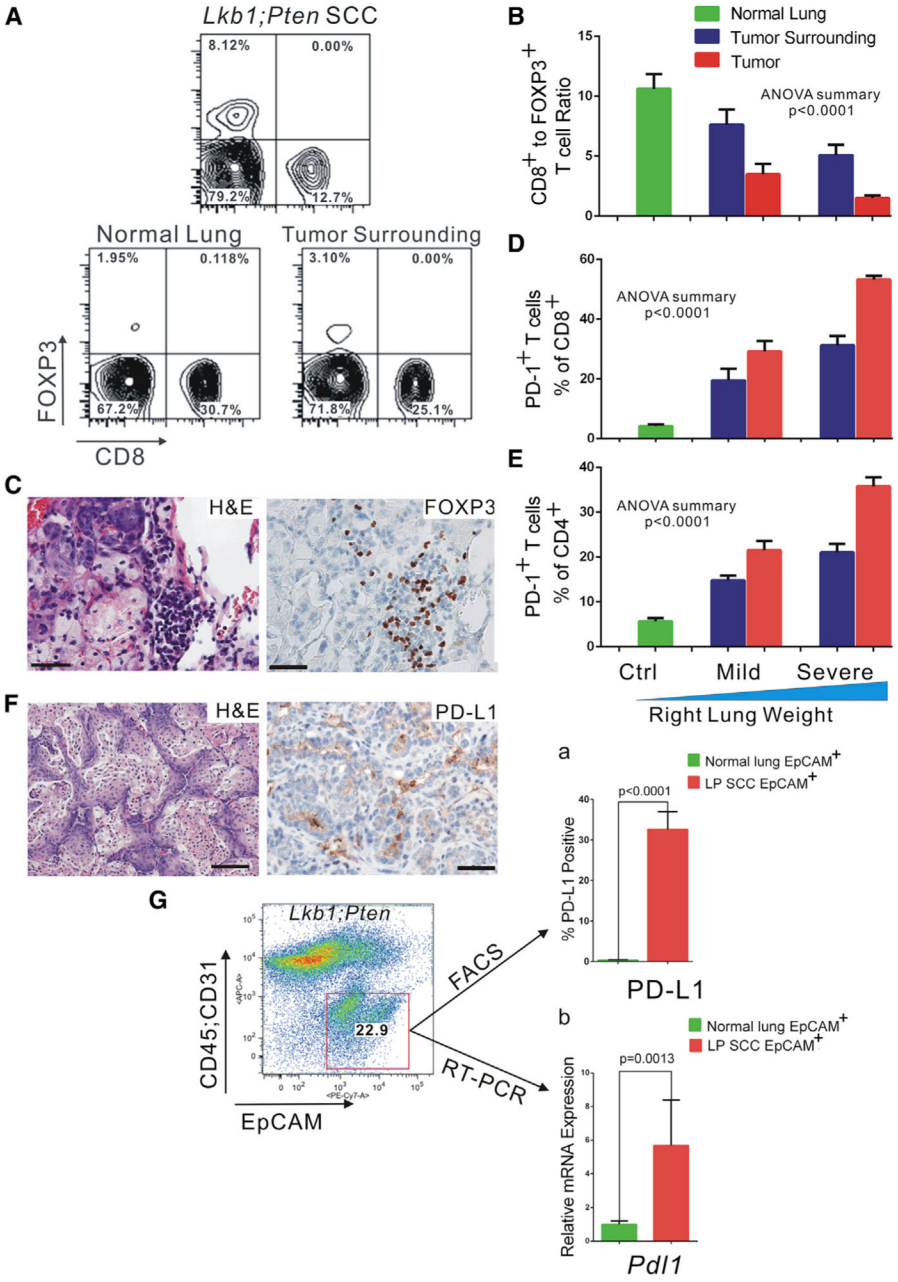

Figure 5. *Lkb1*$^{fl/fl}$;*Pten*$^{fl/fl}$ Lung SCCs Display Hallmarks of Immune Suppression

(A) Representative flow cytometry plots for FOXP3 and CD8 in total CD3$^+$ T cells within LP SCC tumor, uninduced normal lung, and lung surrounding LP SCC tumors.

(B) Ratios of CD8$^+$ T cells to FOXP3$^+$ Tregs as determined with flow cytometry: n = 8 for control lung, n = 5 for mild disease group, and n = 5 for severe disease group ($p < 0.0001$).

(C) Immunohistochemical staining for FOXP3 confirmed the presence of Tregs in LP SCC nodules. Scale bars represent 50 μm for both panels.

(D and E) Quantification the percentage of PD-1 positive cells within the CD8$^+$ (D) and CD4$^+$ (E) T cell populations: n = 8 for control lung, n = 5 for mild disease group, and n = 5 for severe disease group ($p < 0.0001$).

(F) Representative immunohistochemical staining for PD-L1 on LP SCC nodules. Scale bars represent 100 μm for both panels.

(G) (a) Percentage of PD-L1 positive cells within the $EpCAM^{+}CD45^{-}CD31^{-}$ fraction from LP SCC as measured by flow cytometry: n = 7 for LP tumors and n = 5 for normal lung ($p < 0.0001$). (b) Real-time RT-PCR for Pdl1 mRNA levels in the indicated $EpCAM^{+}$ purified cells from SCC tumors and normal lung tissue: n = 6 for normal lung and n = 5 for LP SCC tumors ($p = 0.0013$).

Data are presented as mean ± SEM in (B), (D), (E), and (G). See also Figure S5.

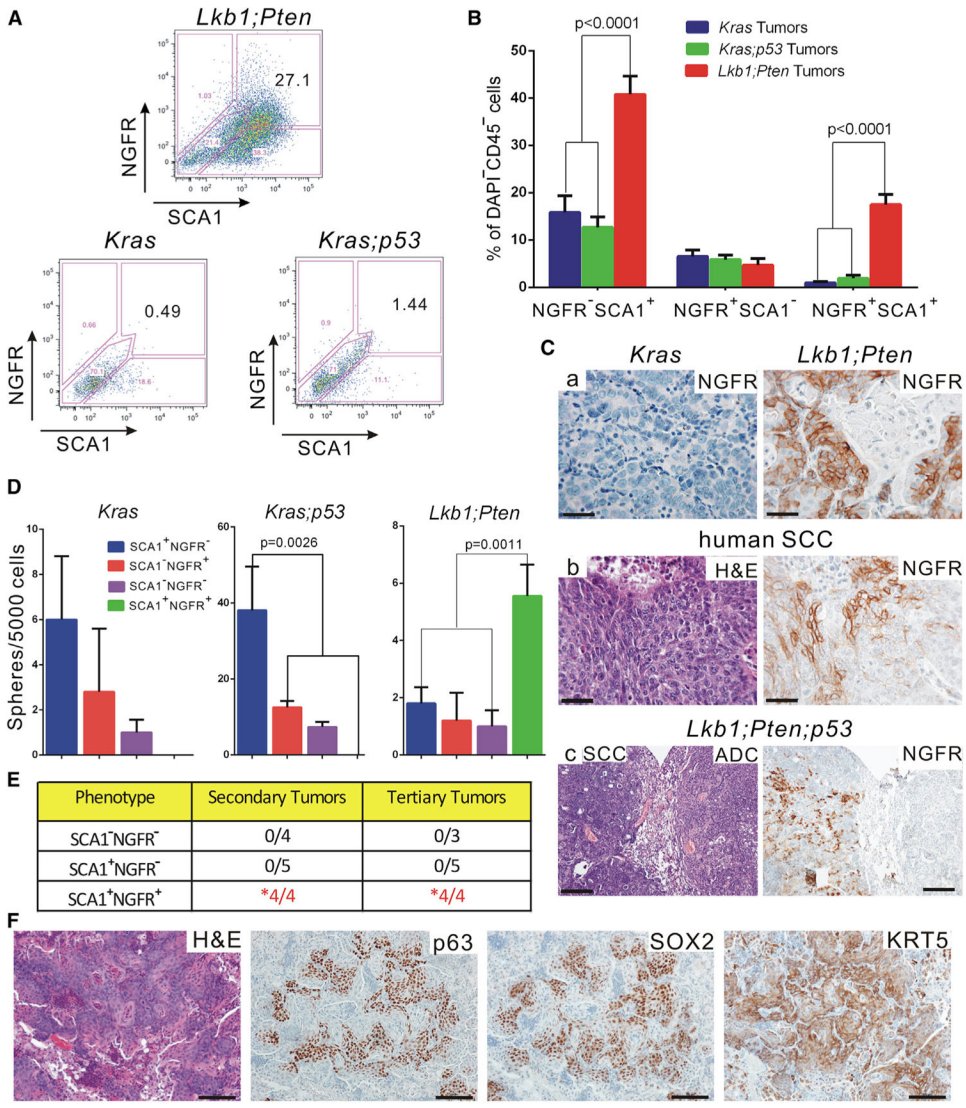

Phenotype	Secondary Tumors	Tertiary Tumors
$SCA1^-NGFR^-$	0/4	0/3
$SCA1^+NGFR^-$	0/5	0/5
$SCA1^+NGFR^+$	*4/4	*4/4

Figure 6. *Lkb1*$^{fl/fl}$;*Pten*$^{fl/fl}$ Lung SCC Contained SCA1$^+$NGFR$^+$ TPCs that Could Serially Transplant Squamous Disease

(A) Representative flow cytometry plots for NGFR and SCA1 expression within the indicated EpCAM$^+$CD45$^-$CD31$^-$ dissociated tumor cell populations. LP tumor cells showed much higher expression of both SCA1 and NGFR than either the *Kras* or *Kras;p53* tumors.

(B) Quantification of SCA1- and NGFR-expressing cells with the EpCAM$^+$CD45$^-$CD31$^-$ population as assessed by flow cytometry. The percentage of SCA1$^+$NGFR$^+$ in LP tumors is much higher than in *Kras* or *Kras;p53* tumors: n = 23 for *Kras* tumors, n = 25 for *Kras;p53* tumors, and n = 34 for *Lkb1;Pten* tumors ($p < 0.0001$).

(C) Representative immunohistochemical staining for NGFR on mouse SCC and ADC (a) and human SCC nodules (b). NGFR staining is strongly positive on SCC tumors but negative on ADC tumors. In the *Lkb1;Pten;p53* tumors, distinct areas of ADC and SCC were adjacently located. NGFR staining was restricted to the SCC area (c). Scale bars represent 50 μm for (a) and (b) and 200 μm for panel (c).

(D) Quantification of tumorspheres derived from $SCA1^{+}NGFR^{+}$, $SCA1^{-}NGFR^{+}$, $SCA1^{+}NGFR^{-}$, and $SCA1^{-}NGFR^{-}$ FACS purified cells that were cocultured in Matrigel with equal amounts of $CD45^{+}CD31^{+}$ cells from the same primary tumors. Each fraction was seeded at 5,000 tumor cells/well. The colony-propagating ability of the $SCA1^{+}NGFR^{+}$ fraction in LP tumors is higher than that of the other fractions ($p = 0.0011$).

(E) Quantification of tumor propagation ability of FACS-isolated $SCA1^{+}NGFR^{+}$, $SCA1^{+}NGFR^{-}$, and $SCA1^{-}NGFR^{-}$ LP tumor cells. The secondary tumors were derived from intratracheal transplantation, with tumor formation latency of ~30 to 40 weeks. The tertiary tumors were derived from intrathoracic injection, with tumor formation latency of ~20 to 30 weeks. Ten thousand sorted cells from each fraction were injected for each fraction and each experiment. Only $SCA1^{+}NGFR^{+}$ populations could form tumors and be serially transplanted ($p = 0.001$ for secondary tumors, $p = 0.002$ for tertiary tumors, Fisher's exact test).

(F) Representative immunohistochemical staining on tertiary tumors derived from $SCA1^{+}NGFR^{+}$ LP tumor cells after intrathoracic injection. The tumors retained a squamous histology and were positive for all of the squamous markers examined. Scale bars represent 100 μm for all panels.

Data are presented as mean ± SEM in (B) and (D). See also Figure S6.

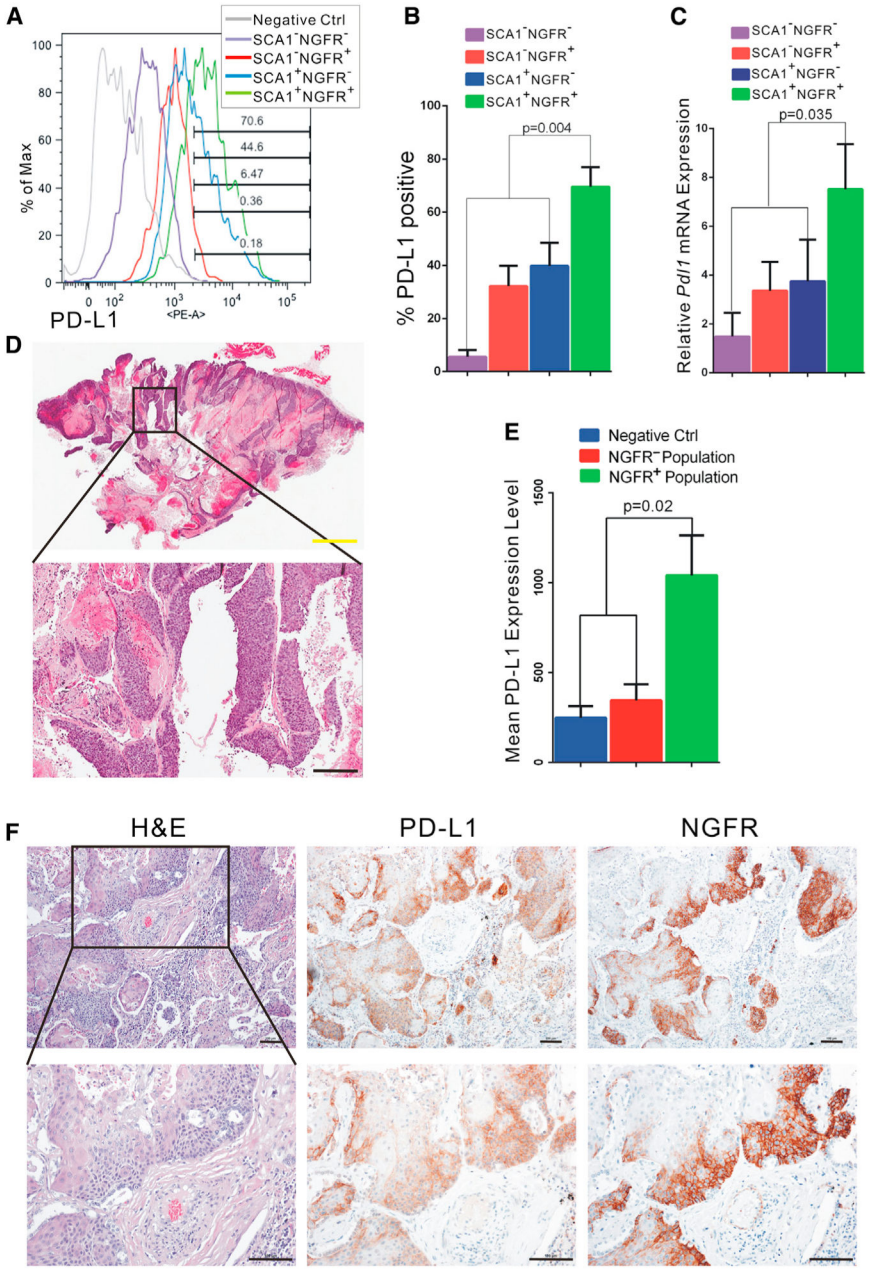

Figure 7. SCA1^{+}NGFR^{+} TPCs in *Lkb1*$^{fl/fl}$;*Pten*$^{fl/fl}$ Lung SCC Tumor Expressed High Levels of PD-L1

(A) Representative histogram of PD-L1 expressing cells from a dissociated LP tumor gated on DAPI^{-}EpCAM^{+}CD45^{-}CD31^{-} cells and then for the four indicated fractions of SCA1;NGFR-expressing cells. The unstained control trace in gray is shown for gating. DAPI, 4′,6-diamidino-2-phenylindole.

(B) Quantification of PD-L1 expression level by flow cytometric analysis. PD-L1 expression is higher in SCA1^{+}NGFR^{+} population than any other population (n = 7 tumors, p = 0.004).

(C) Real-time RT-PCR quantification of *Pdl1* mRNA expression in $SCA1^{+}NGFR^{+}$, $SCA1^{-}NGFR^{+}$, $SCA1^{+}NGFR^{-}$, and $SCA1^{-}NGFR^{-}$ sorted populations (n = 7 tumors, p = 0.035).
(D) Representative H&E staining confirming that PDX tumors retained squamous histology. The black scale bar represents 200 μm, and the yellow scale bar represents 2,000 μm.
(E) Quantification of PD-L1 expression level by flow cytometric analysis of PDX samples. Mean fluorescence intensities for PD-L1 antibody on $EpCAM^{+}NGFR^{+}$ fractions are higher than those for $EpCAM^{+}NGFR^{-}$ fractions. The control is unstained dissociated PDX cells (n = 6 tumors, p = 0.02).
(F) Serial sections of formalin-fixed human SCC tumors stained with H&E, PD-L1, or NGFR. PD-L1 is colocalized to the $NGFR^{+}$ cells within these tumors. Scale bars represent 100 μm for all panels.
Data are presented as mean ± SEM in (B), (C), and (E). See also Figure S7.